of 90–92% purity with contamination of ca. 2–4% P_4S_7 and ca. 4–8% β-P_4S_5 (see Experimental Section). The ^{31}P MAS spectra of the two β-P_4S_6 polymorphs are depicted in Figure 7. For β-P_4S_6(A) (e.g., Figure 7a) we identify four resonances of approximately equal intensity and with centerbands at 210.6 (singlet, P4), 191.9 (doublet, P1 or P2), 183.9 (doublet, P1 or P2), and 65.2 ppm (singlet, P3). The assignment follows from the 1D and 2D spectra of the melt containing β-P_4S_6 and from the doublet splittings assigned to $^1J(P1,P2) = 320 \pm 10$ Hz (observed at both 7.1 and 9.4 T). Thus, for β-P_4S_6(A) P1 and P2 are also inequivalent due to crystal-packing effects. From the different intensities of the centerbands and ssb's for P1 and P2 in Figure 7a it is obvious that their shielding tensor elements differ and are quite sensitive to crystal packing.

For the ^{31}P MAS spectra of β-P_4S_6(B) (e.g., Figure 7b) a 17-ppm shift toward greater shielding for the P4 singlet relative to its chemical shift in β-P_4S_6(A) is observed. It thereby coincides with the high-frequency doublet (P1 or P2) observed at 192.0 ppm. The other P1/P2 doublet is observed at 178.6 ppm. Thus, the following four resonances are identified for β-P_4S_6(B): 193.7 (singlet, P4), 192.0 (doublet, P1 or P2), 178.6 (doublet, P1 or P2), and 70.4 (singlet, P3). Most remarkably the doublet splitting for β-P_4S_6(B), $^1J(P1,P2) = 225 \pm 15$ Hz, is reduced by about 100 Hz compared to the value observed for β-P_4S_6(A) but is comparable to $^1J(P1,P2)$ for P_4S_7 and β-P_4S_5(B). We have presently no explanation for the differences in the magnitudes of $^1J(P1,P2)$ for the two polymorphs of β-P_4S_6. A single-crystal X-ray study of β-P_4S_6(B) (large crystals) shows that the asymmetric unit is one entire molecule ($P1_1/c$, $Z = 4$)[16] consistent with the observation of four resonances in the ^{31}P MAS spectrum.

Concluding Remarks

In conclusion, high-temperature 1D and 2D ^{31}P NMR spectroscopy is shown to be an efficient tool for studying molecular transformations and exchange pathways in melts of β-P_4S_5 or of mixtures of P_4S_3 and sulfur. These studies facilitate chemical shift assignments of earlier incorrectly assigned, unassigned, or unknown solution-state ^{31}P NMR spectra of P_4S_n compounds. Furthermore, the 2D exchange studies in the molten state greatly assist the interpretation of solid-state NMR investigations of P_4S_n compounds. The ability of solid-state ^{31}P MAS–NMR to distinguish and identify new polymorphs and isomers in the series of P_4S_n (n = 5 and 6) compounds is demonstrated. Its sensitivity to crystal-packing effects, not obvious from X-ray diffraction, is illustrated to be an important factor in this respect. Such effects lead to observation of ^{31}P–^{31}P scalar couplings which cannot be determined for the "free" molecules in solution or melt because the P atoms become equivalent due to symmetry.

Acknowledgment. The use of the facilities at the University of Aarhus NMR Laboratory sponsored by the Danish Research Councils SNF and STVF, Carlsbergfondet, and Direktør Ib Henriksens Fond is acknowledged. We thank Aarhus University Research Foundation for equipment grants.

High-Resolution Oxygen-17 NMR of Solid Silicates

K. T. Mueller, Y. Wu, B. F. Chmelka, J. Stebbins,† and A. Pines*

Contribution from the Materials and Chemical Sciences Division, Lawrence Berkeley Laboratory, 1 Cyclotron Road, Berkeley, California 94720, and Department of Chemistry, University of California, Berkeley, California 94720. *Received June 1, 1990*

Abstract: Several ^{17}O-enriched silicates were studied by use of dynamic angle spinning (DAS) and double rotation (DOR) nuclear magnetic resonance spectroscopy. These methods average away second-order quadrupolar interactions by reorienting a sample about a time-dependent axis, thereby yielding high-resolution spectra of oxygen-17 nuclei. A narrow spectral line is observed for each distinct oxygen site at the sum of the isotropic chemical shift and the field-dependent isotropic second-order quadrupolar shift. Resolution is increased by up to 2 orders of magnitude compared to conventional magic angle spinning (MAS) spectra. Crystallographically inequivalent oxygens are now observable as distinct resonances in spectra of polycrystalline silicates such as diopside ($CaMgSi_2{}^{17}O_6$), wollastonite ($CaSi^{17}O_3$), clinoenstatite ($MgSi^{17}O_3$), larnite ($Ca_2Si^{17}O_4$), and forsterite ($Mg_2Si^{17}O_4$).

Introduction

Solid silicates display an array of structures and phases according to their composition and thermal treatment. As the molar percentage of cations increases, for example, the infinite three-dimensional framework of crystalline silica (SiO_2) gives way to more compact chains of Si–O atoms (pyroxenes and amphiboles) and discrete anionic species (orthosilicates and cyclosilicates). Such variations in microstructure can have significant impact on the macroscopic properties of silicate species.[1] Adsorption and reaction processes of porous aluminosilicates, such as zeolites, are tied closely to their local structure, influencing their use as catalysts, selective adsorbents, and ion-exchange media in a variety of important industrial processes.[2] Furthermore, the abundance of silicon and oxygen in the Earth's crust[3] makes physicochemical studies of solid silicates important for understanding many natural geochemical processes.

The microstructure of silicates can be probed by examining the electromagnetic environment of their nuclei with the use of nuclear magnetic resonance (NMR) spectroscopy. Nearby electrons influence the local magnetic field at the nucleus by both paramagnetic and diamagnetic mechanisms, so that measurement of the shielding (chemical shift) tensor at a specific site is a sensitive probe of the local bonding.[4] A nucleus with a nonspherical charge

* To whom correspondence should be addressed at the University of California.

† Address: Department of Geology, Stanford University, Stanford, CA 94305.

(1) Deer, W. A.; Howie, R. A.; Zussman, J. *Rock-Forming Minerals*; Halsted Press: New York, 1978; Vols. 1, 2.

(2) Breck, D. W. *Zeolite Molecular Sieves: Structure, Chemistry and Use*; Robert E. Krieger: Malabar, FL, 1984.

(3) Douglas, B.; McDaniel, D. H.; Alexander, J. J. *Concepts and Models of Inorganic Chemistry*, 2nd ed.; Wiley: New York, 1983; pp 237–241.

(4) Kirkpatrick, R. J. In *Spectroscopic Methods in Mineralogy and Geology*; Mineralogical Society of America, Reviews in Mineralogy; Hawthorne, F. C., Ed.; Mineralogical Society of America: Washington, D.C., 1988; Vol. 18, pp 341–403 and references therein.

0002-7863/91/1513-32$02.50/0

distribution couples additionally to local electric field gradients through the electric quadrupole interaction.[5-8] Determination of the strength of the quadrupolar coupling and the deviation of the electric field gradient from axial symmetry provides additional structural insight because the interaction is also dependent upon bonding and symmetry of the local atomic environment.

High-field NMR has been used to study silicates, focusing primarily on the silicon-29 nucleus,[9-11] which, like carbon-13, is a low-abundance spin-$^1/_2$ isotope. Line broadening in silicon spectra is caused predominantly by anisotropy of the chemical shift and may be removed by use of magic angle spinning (MAS) NMR.[12-16] High-resolution spectra can be obtained in this way,[17] often yielding quantitative structural information. High-resolution oxygen-17 NMR studies of silicates, however, are much more difficult as a result of quadrupolar couplings of the oxygen-17 nuclei.

Oxygen has a nuclear spin $I = {}^5/_2$, so all single quantum ($\Delta m = 1$) spin transitions other than the central ($^1/_2 \leftrightarrow -^1/_2$) transition are broadened by first-order quadrupolar interactions (except in highly symmetric crystalline environments). One normally detects the central transition in which second-order quadrupolar effects must often be taken into account. In a polycrystalline or amorphous sample, NMR resonances are broadened by the spatial anisotropy of the second-order interaction, which cannot be fully averaged by MAS methods.[18,19] Individual spectral lines from distinct oxygen-17 nuclear environments typically overlap, and the separation and identification of different oxygen sites is difficult.

Recent developments have allowed an increase in NMR spectral resolution by up to 2 orders of magnitude for quadrupolar nuclei. The techniques of dynamic angle spinning (DAS) and double rotation (DOR) average second-order effects by reorienting the axis of a rapidly rotating powdered sample through a time-dependent trajectory during a pulsed NMR experiment.[20-23] Preliminary use of these techniques to study oxygen in minerals has provided narrowed resonances and increased spectral resolution.[22] Here, we present new DAS and DOR results from a number of silicate minerals, including pyroxenes and orthosilicates, in which individual resonances are now detected for crystallographically distinct oxygen species. The resolution of oxygen sites in these samples bodes well for the study of other oxygen-containing materials such as polymers and ceramic superconductors.

Second-Order Averaging by DAS and DOR

Central-transition line shapes and relative peak positions in high-field NMR spectra of quadrupolar nuclei are determined by the chemical shift tensor, the quadrupolar coupling constant (C_Q), and the asymmetry parameter of the electric field gradient (η) at each nuclear site. A powdered sample contains many crystallites with different orientations of the principle axis system (PAS) of the electric field gradient with respect to the external magnetic field. For each distinct nuclear site, the sum of the resonance frequencies from crystallites in all possible orientations results in a broad powder pattern. Each pattern is centered at its isotropic frequency, appearing at the sum of the isotropic chemical shift and the isotropic component of the second-order quadrupolar interaction.

Spinning the sample about a fixed axis in space reduces the line widths by a factor of 3–4 (refs 19 and 24) by partially averaging the anisotropic part of the second-order quadrupolar interaction. In the limit of a spinning speed sufficiently fast to separate any spinning sidebands from the central-transition powder pattern, the anisotropic frequency for a crystallite oriented at polar angles α' and β' with respect to a spinner axis inclined at an angle θ to the external field is

$$\nu_{aniso} = A\sum_{i=0}^{2}\sum_{j=0}^{2} a_{ij} \cos(2i\alpha') \cos(2j\beta') \quad (1)$$

with

$$a_{ij} = a_{ij}^{(2)}P_2(\cos\theta) + a_{ij}^{(4)}P_4(\cos\theta) \quad (2)$$

The quantities $a_{ij}^{(l)}$ for $l = 2$ and 4, as well as the constant A, are found in Table I. The second and fourth Legendre polynomials are given by

$$P_2(\cos\theta) = \tfrac{1}{2}(3\cos^2\theta - 1) \quad (3)$$

$$P_4(\cos\theta) = \tfrac{1}{8}(35\cos^4\theta - 30\cos^2\theta + 3) \quad (4)$$

The resulting NMR powder pattern is calculated by averaging over all orientations in a powdered sample. The observed center of mass of the powder pattern is shifted from the zeroth-order Larmor frequency (ν_L) by an amount (in ppm)

$$\delta_{obs} = \delta_{iso}{}^{CS} + \delta_{iso}{}^{(2)} \quad (5)$$

where $\delta_{iso}{}^{CS}$ is the isotropic chemical shift. The isotropic second-order quadrupolar shift in frequency units is

$$\nu_{iso}{}^{(2)} = -\frac{3}{40}\frac{C_Q{}^2(I(I+1) - \frac{3}{4})}{\nu_L I^2(2I-1)^2}\left(1 + \frac{1}{3}\eta^2\right) \quad (6)$$

with quadrupolar coupling constant

$$C_Q = \frac{e^2qQ}{h} \quad (7)$$

The quantity eQ is the nuclear electric quadrupole moment (−2.6

Table I. Coefficients in the Anisotropic Frequency Cosine Expansion

$$\nu_{1/2\leftrightarrow -1/2}^{(2)} = \nu_{iso}^{(2)} + A\sum_{i=0}^{2}\sum_{j=0}^{2} a_{ij} \cos(2i\alpha') \cos(2j\beta')$$

$$A = \left(\frac{C_Q}{2I(2I-1)}\right)^2 \frac{4I(I+1) - 3}{32\nu_L}$$

$$a_{ij} = a_{ij}^{(4)}P_4(\cos\theta) + a_{ij}^{(2)}P_2(\cos\theta)$$

i	j	$a_{ij}^{(4)}$	$a_{ij}^{(2)}$
0	0	$81/1120(18 + \eta^2)$	$-12/7(1 - \eta^2/3)$
0	1	$9/56(18 + \eta^2)$	$-36/7(1 - \eta^2/3)$
0	2	$9/32(18 + \eta^2)$	0
1	0	$81\eta/56$	$24\eta/7$
1	1	$27\eta/14$	$-24\eta/7$
1	2	$-27\eta/8$	0
2	0	$27\eta^2/32$	0
2	1	$-9\eta^2/8$	0
2	2	$9\eta^2/32$	0

(5) Pound, R. V. *Phys. Rev.* **1950**, *79*, 685–702.
(6) Cohen, M. H.; Reif, F. *Solid State Physics* **1957**, *5*, 321–438.
(7) Volkoff, G. M. *Can. J. Phys.* **1953**, *31*, 820–836.
(8) Narita, K.; Umeda, J.-I.; Kusumoto, H. *J. Chem. Phys.* **1966**, *44*, 2719–2723.
(9) Lippmaa, E.; Mägi, M.; Samoson, A.; Engelhardt, G.; Grimmer, A.-R. *J. Am. Chem. Soc.* **1980**, *102*, 4889–4893.
(10) Mägi, M.; Lippmaa, E.; Samoson, A; Engelhardt, G.; Grimmer, A.-R. *J. Phys. Chem.* **1984**, *88*, 1518–1522.
(11) Grimmer, A.-R.; von Lampe, F.; Mägi, M. *Chem. Phys. Lett.* **1986**, *132*, 549–553.
(12) Andrew, E. R.; Bradbury, A.; Eades, R. G. *Nature (London)* **1958**, *182*, 1659.
(13) Schaefer, J.; Stejskal, E. O. *J. Am. Chem. Soc.* **1976**, *98*, 1031–1032.
(14) Fyfe, C. A. *Solid State NMR for Chemists*; CFC Press: Guelph, 1983.
(15) Maciel, G. E. *Science* **1984**, *226*, 282–288.
(16) Maricq, M. M.; Waugh, J. S. *J. Chem. Phys.* **1979**, *70*, 3300–3316.
(17) Fyfe, C. A.; O'Brien, J. H.; Strobl, H. *Nature (London)* **1987**, *326*, 281–283.
(18) Kundla, E.; Samoson, A.; Lippmaa, E. *Chem. Phys. Lett.* **1981**, *83*, 229–232.
(19) Samoson, A.; Kundla, E.; Lippmaa, E. *J. Magn. Reson.* **1982**, *49*, 350–357.
(20) Llor, A.; Virlet, J. *Chem. Phys. Lett.* **1988**, *152*, 248–253.
(21) Samoson, A.; Lippmaa, E.; Pines, A. *Mol. Phys.* **1988**, *65*, 1013–1018.
(22) Chmelka, B. F.; Mueller, K. T.; Pines, A.; Stebbins, J.; Wu, Y.; Zwanziger, J. W. *Nature (London)* **1989**, *339*, 42–43.
(23) Mueller, K. T.; Sun, B. Q.; Chingas, G. C.; Zwanziger, J. W.; Terao, T.; Pines, A. *J. Magn. Reson.* **1990**, *86*, 470–487.
(24) Ganapathy, S.; Schramm, S.; Oldfield, E. *J. Chem. Phys.* **1982**, *77*, 4360–4365.

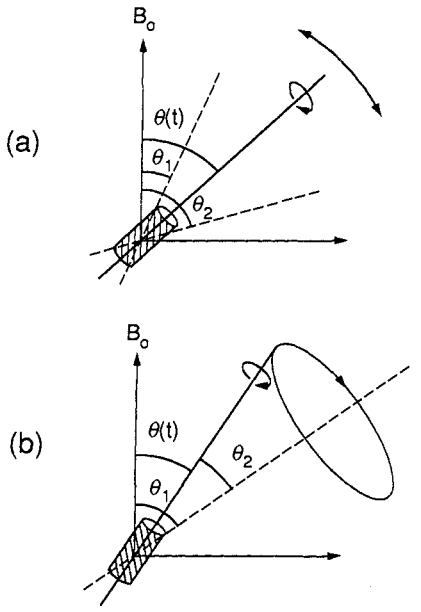

Figure 1. Schematic representation of the two approaches for averaging second-order interactions: (a) dynamic angle spinning and (b) double rotation.

$\times 10^{-30}$ m^2 for oxygen-17); eq is the z-component of the electric field gradient at the nucleus; η is the asymmetry parameter of the electric field gradient; and h is Planck's constant. The magnitudes of both the anisotropy (or the overall width of the pattern) and the isotropic second-order frequency shift scale with the inverse of ν_L. Therefore, it is preferable to work at high fields to minimize these effects and improve spectral resolution.

It is now clear why magic angle spinning (where $\theta = 54.74°$, the root of $P_2(\cos\theta)$) will not completely narrow the lines in the NMR spectra of quadrupolar species. The dependence of the frequency on $P_4(\cos\theta)$ in eq 2 leaves a broadened spectrum after averaging over α' and β'. In fact, no single angle may be chosen so that both $P_2(\cos\theta)$ and $P_4(\cos\theta)$ are simultaneously zero. Since second-order effects are neither small at the magnetic field strengths currently available nor completely averaged by any simple (single-axis) mechanical reorientation, it is necessary to reorient the sample about at least two axes.

Dynamic angle spinning utilizes a spinning sample whose axis is flipped rapidly from one angle to another with respect to the magnetic field B_0 (Figure 1a). In this version of spinning about two axes, two DAS complementary angles, θ_1 and θ_2, are selected so that

$$P_2(\cos\theta_1) = -kP_2(\cos\theta_2) \quad (8)$$

$$P_4(\cos\theta_1) = -kP_4(\cos\theta_2) \quad (9)$$

Spinning first for a time τ_1 at angle θ_1 and then for a time $\tau_2 = k\tau_1$ at θ_2 will cause the evolution of the spin system to appear isotropic (i.e., independent of orientation) when the magnetization is measured at a time $t_1 = \tau_1 + \tau_2$. Spectral lines then appear at the isotropic frequencies (eqs 5 and 6) for each spin. This averaging, or refocusing, permits resolution of overlapping resonances because the isotropic components are narrow and their maxima occur at orientation-independent frequencies. Two-dimensional NMR is useful, but not necessary, to obtain high-resolution DAS spectra, since it correlates the isotropic peaks with the broadened signals obtained under single-axis rotation at the angle θ_2. Information concerning the anisotropies is still present in this second dimension.

There is a continuum of solutions for the angles in a DAS experiment, bounded by 0° and 39.23° for one angle (θ_1) and 63.43° and 90° for the second angle (θ_2). Figure 2 presents the solutions graphically as a function of the parameter k, the ratio of evolution time at the second angle to time spent at the first angle in the experiment. Our choice of angles (θ_1, θ_2) has been for $k = 1$ (37.38°, 79.19°), but equally valid are the pairs (0.00°,

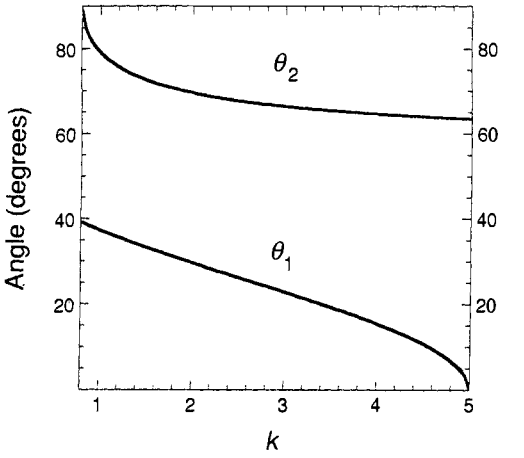

Figure 2. Complementary angles as a function of the ratio of time spent at each angle during the t_1 dimension of a DAS experiment.

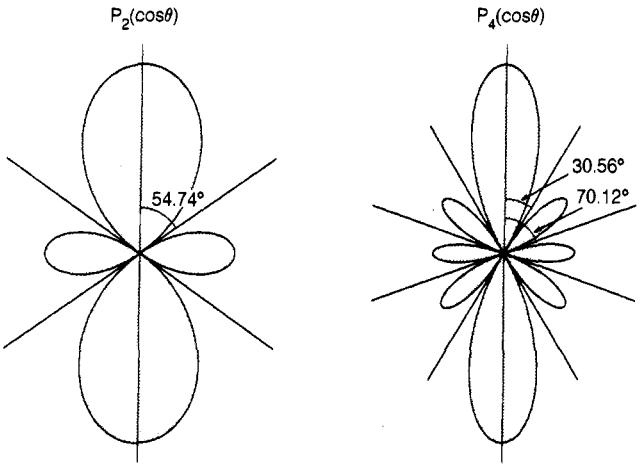

Figure 3. Polar graphs of the functions $P_2(\cos\theta)$ and $P_4(\cos\theta)$ reveal the magic angles used in the DOR experiment: 54.74° and either 30.56° or 70.12°.

63.43°), (30.56°, 70.12°), and (39.23°, 90.00°), with k equal to 5, 1.87, and 0.8, respectively.

Double rotation is a continuous or parallel version of the two-axis sample reorientation strategy, in which one spinning axis precesses about another (Figure 1b). In this case, the anisotropic frequency contribution for a crystallite is given by

$$\nu_{aniso} = B \sum_{l=2,4} A_l(\alpha',\beta') P_l(\cos\theta_1) P_l(\cos\theta_2) \quad (10)$$

where the constant B is related to the strength of the quadrupolar coupling and spin of the nucleus. The A_l terms are functions of the orientation of crystallites with respect to the spinning axes.

To average the anisotropies at all times during the DOR experiment, the angles θ_1 and θ_2 must be zeros of the second and fourth Legendre polynomials (Figure 3). In practice,[25] a powdered sample in a small rotor is spun inside a larger rotor whose spinning axis is inclined at the magic angle (54.74°) with respect to the external field. The small rotor has its spinning axis oriented at a higher order magic angle (30.56°, a zero of $P_4(\cos\theta)$) with respect to the spinning axis of the large rotor.

In both DAS and DOR, the frequency measured is the sum of an isotropic chemical shift and a field-dependent isotropic second-order shift, and it is useful to separate these two contributions in order to determine the values of δ_{iso}^{CS}, C_Q, and η. Since the quadrupolar shift is proportional to the inverse of the magnetic field strength, performing an experiment at two or more field strengths will allow determination of the isotropic chemical shift for each site. Alternatively, the quadrupolar parameters (C_Q and

(25) Samoson, A.; Pines, A. *Rev. Sci. Instrum.* **1989**, *60*, 3239–3241.

η) may be determined from the second dimension in a DAS experiment by simulations of resolved powder patterns at isotropic positions in the first dimension.

Experimental Section

Sample Preparation. All silicate compounds were synthesized from ^{17}O-enriched SiO_2, CaO, and MgO precursor compounds prepared from reaction of $H_2{}^{17}O$ with the proper inorganic starting materials.[26] $Si^{17}O_2$ was produced by reacting liquid $H_2{}^{17}O$ with $SiCl_4$ vapor at ambient temperature and pressure, followed by dehydration of the product at 1473 K. $Ca(^{17}OH)_2$ was synthesized by direct oxidation of calcium metal with $H_2{}^{17}O$ under ambient conditions in an argon glovebox, with $Ca^{17}O$ produced by drying the hydroxide at 853 K. Reacting saturated solutions of $K^{17}OH$ and $MgCl_2$ at 298 K precipitated $Mg(^{17}OH)_2$, which yielded $Mg^{17}O$ upon decomposition at 653 K.

The simple oxide products were mixed together in the proper stoichiometric amounts, heated to elevated temperatures in sealed Pt tubes or in an N_2 atmosphere, and cooled to ambient conditions to produce homogeneous crystalline phases of diopside ($CaMgSi_2{}^{17}O_6$), forsterite ($Mg_2Si^{17}O_4$), larnite ($Ca_2Si^{17}O_4$), clinoenstatite ($MgSi^{17}O_3$), and wollastonite ($CaSi^{17}O_3$). Ultimate enrichments of oxygen-17 were 20% in the diopside, 41% in the wollastonite and clinoenstatite, and 43% in the larnite and forsterite. Phase identity was checked by powder X-ray diffraction and silicon-29 NMR. The forsterite sample was slightly off stoichiometry and contained approximately 25% clinoenstatite.

NMR Experiments. Experiments were performed in a magnetic field of 9.4 T, corresponding to an oxygen-17 resonance frequency of 54.25 MHz. The probe heads for the sample reorientation were machined from commercially available Delrin and Vespel polymers. The DOR probe head has been described in detail elsewhere.[27] The DAS probe head is a new version, improved from that used in previous experiments,[23] and it is described in ref 28.

The DAS experiments were performed as detailed in ref 23, with axis flips from $\theta_1 = 37.4°$ to $\theta_2 = 79.2°$ and appropriate phase cycling of the radio frequency pulses. For these angles, the evolution times at the two angles must be equal in order to cancel the anisotropic frequency contributions. Eight experiments are necessary to reconstruct a full second-order quadrupolar echo that is digitized starting from the point of refocusing. The second time dimension (t_2) contains the digitized data after refocusing of first- and second-order anisotropic interactions, and its Fourier transform provides the spectrum of the sample while spinning at θ_2. The first time dimension (t_1) is the sum of the two evolution times leading to the anisotropic refocusing. This first dimension is incremented by a time Δt_1 (typically tens of microseconds), and the anisotropic decay during t_2 is recorded for each t_1 delay. The spectral width in the second frequency dimension is the inverse of the sampling period between data points in the second time dimension, while the spectral width in the first frequency dimension is $1/\Delta t_1$.

One-dimensional DAS spectra are obtained by a Fourier transformation of the echo heights as a function of the first time dimension. This yields resolved lines with quantitative peak intensities after assignment and integration of all spinning sidebands. All two-dimensional DAS spectra are presented in absolute-value mode to avoid phase-twisted line shapes.[29,30] Projections along the first frequency axis also provide high-resolution results, though some additional line broadening occurs owing to the absolute value calculation. Pure absorption mode DAS experiments are also possible, reducing line widths in the two-dimensional spectra and allowing correlation with magic angle spinning powder patterns in the second dimension. These will be reported in a future communication.[31]

A DOR spectrum, while technically more demanding, is acquired in a one-pulse NMR experiment, which provides high-resolution spectra with fewer signal acquisitions than in the DAS experiment. Fourier transformation of a conventional one-dimensional FID gives the high-resolution spectrum immediately. Comparison of spectra obtained at a variety of spinning speeds can help in the assignment of sidebands arising from the larger (outer) rotor. DAS spectra also contain sidebands (at integer multiples of half of the rotor frequency), but since the spinning speeds used here are on the order of many kilohertz, this rarely complicates analysis of the data. Used together, these two techniques provide complementary information and unambiguous peak identification.

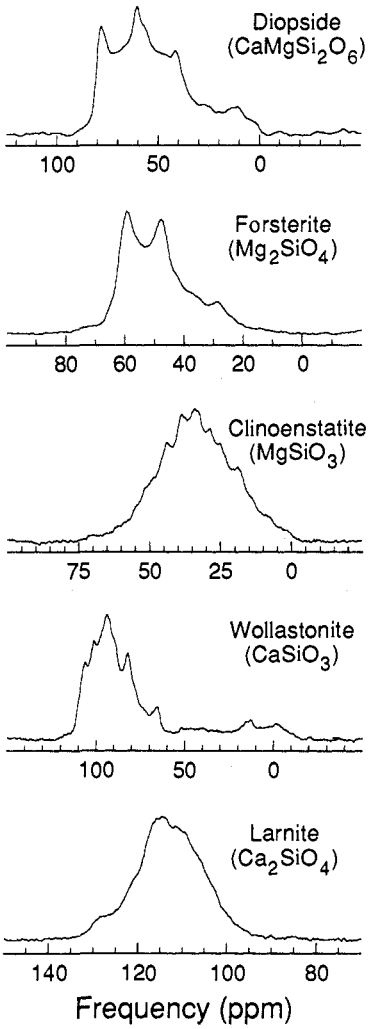

Figure 4. Magic angle spinning spectra of five silicate minerals at an oxygen-17 resonance frequency of 54.25 MHz (9.4 T), with spinning frequencies of 5.4 kHz. The resonance frequency of oxygen-17 in 37.5% enriched $H_2{}^{17}O$ is the zero of each frequency axis.

Table II. Previously Determined Oxygen-17 Chemical Shift ($\delta_{iso}{}^{CS}$) and Quadrupolar Parameters (C_Q and η) for Three Silicates, Based on Three-Site Models

compd	ref	site[a]	occ	$\delta_{iso}{}^{CS}$ (ppm)	C_Q (MHz)	η	$\delta_{obs}{}^{c}$ (ppm)
diopxide ($CaMgSi_2O_6$)	33	nb	1	84	2.7	0.0	69
		nb	1	63	2.7	0.1	48
		br	1	69	4.4	0.3	28
forsterite[b] (Mg_2SiO_4)	32	a	2	61	2.35	0.2	50
		b	1	62	2.35	1.0	47
		c	1	47	2.7	0.3	32
clinoenstatite	33	nb	1	60	3.2	0.0	39
($MgSiO_3$)		nb	1	42	3.2	0.0	21
		br	1	62	5.1	0.3	7

[a] The designations nb and br signify nonbridging and bridging oxygen sites, respectively. [b] For forsterite, all three sites are nonbridging. [c] The calculated total isotropic shifts (δ_{obs}) at 9.4 T (see eqs 5 and 6).

Results

Typical MAS spectra for oxygen-17 in some minerals are shown in Figure 4; powder patterns from distinct oxygen sites overlap at a field strength of 9.4 T. Diopside, forsterite, and clinoenstatite have been investigated previously[32,33] with analyses assuming the presence of three inequivalent oxygen sites. Spectra were simulated

(26) Chmelka, B. F. Ph.D. Thesis, University of California, Berkeley, May, 1990.
(27) Wu, Y.; Sun, B. Q.; Pines, A.; Samoson, A.; Lippmaa, E. *J. Magn. Reson.* **1990**, *89*, 297–309.
(28) Mueller, K. T.; Chingas, G. C.; Pines, A. *Lawrence Berkeley Lab., LBL* LBL29042, to be submitted for publication.
(29) States, D. J.; Haberkorn, R. A.; Ruben, D. J. *J. Magn. Reson.* **1982**, *48*, 286–292.
(30) Keeler, J.; Neuhaus, D. *J. Magn. Reson.* **1985**, *63*, 454–472.
(31) Mueller, K. T.; Wooten, E. W.; Pines, A. *J. Magn. Reson.*, in press.
(32) Schramm, S.; Oldfield, E. *J. Am. Chem. Soc.* **1984**, *106*, 2502–2506.
(33) Timken, H. K. C.; Schramm, S. E.; Kirkpatrick, R. J.; Oldfield, E. *J. Phys. Chem.* **1987**, *91*, 1054–1058.

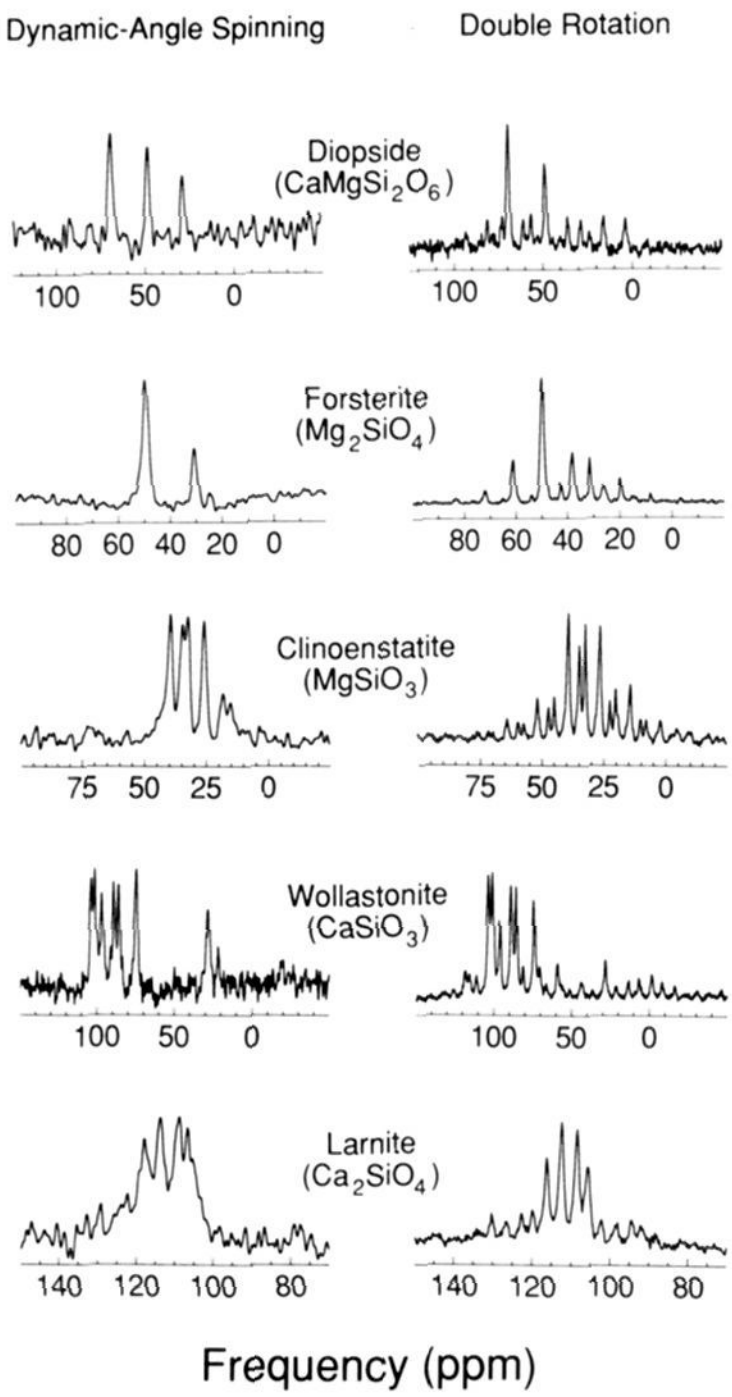

Figure 5. Oxygen-17 DAS and DOR spectra at 54.25 MHz. For all DAS experiments, the rotor frequencies are 5.4 kHz. In the DOR experiments, the inner rotor spins at 5 kHz, while the outer rotates at approximately 800 Hz. The experimentally observed shifts with respect to $H_2{}^{17}O$ are compiled in Table III.

by fitting the experimental NMR line shapes to computer-generated powder patterns, and the isotropic chemical shifts and quadrupolar parameters obtained are shown in Table II. A difference in the magnitude of C_Q for bridging versus nonbridging oxygen sites is observed, and this is attributed to the difference in ionicity of cation–oxygen bonds in the two arrangements. The more ionic bonds associated with the terminal oxygens result in less p-orbital contribution to the electric field gradient[33] and thus a lower quadrupolar coupling frequency. Equations 5 and 6, furthermore, allow calculation of the total observed shifts expected at 9.4 T, and these are included in Table II as well.

DAS and DOR spectra of the same silicate materials are shown in Figure 5. Isotropic shifts are distinguished from spinning sidebands by performing experiments at two or more spinning speeds and by comparison of the DAS and DOR spectra for each material. Due to the presence of many peaks in some of the spectra, labeling of the isotropic peaks and sidebands would add confusion to the presentation of the results, so the observed values are compiled in Table III.

The DAS and DOR results for diopside and forsterite agree with models having three distinct oxygen sites. This is consistent with their reported crystal structures[34,35] shown in Figure 6a,b. The quadrupolar parameters and isotropic chemical shifts, determined from previous MAS experiments,[32,33] predict observed shifts in excellent quantitative agreement with the new experimental values. The three resonances are fully resolved in the diopside spectra, with their integrated intensities reflecting a 1:1:1 oxygen site occupancy. Analysis of the forsterite data is less straightforward due to partial overlap of the narrowed peaks from two oxygen-17 sites. Expansion of the region around the most intense peak in the DOR spectrum (Figure 7) reveals a shoulder on the resonance from a third oxygen site. Comparison with the MAS spectra at 11.7 T (ref 32) strengthens the conclusion that three main sites are present. Moreover, the enhanced resolution permits impurity phases to be detected, as evidenced by the small peak at 26 ppm in both DAS and DOR spectra. We attribute this to an impurity in the polycrystalline forsterite, also detected by X-ray diffraction and silicon-29 NMR.[36] Its identification

(34) Warren, B.; Bragg, W. L. *Z. Kristallogr.* **1928**, *69*, 168–193.
(35) Wyckoff, R. W. G. *Crystal Structures*; Interscience Publishers: New York, 1948; Vol. 3, Chapter 12, pp 5–9.

Table III. Experimentally Determined Oxygen-17 Shifts at 9.4 T

compd	$\delta_{obs}{}^a$ (ppm)	compd	$\delta_{obs}{}^a$ (ppm)
diopside ($CaMgSi_2O_6$)	69.2	wollastonite ($CaSiO_3$)	103.4
	48.5		100.1
	28.6		96.5
forsterite (Mg_2SiO_4)	49.0		89.0
	49.0		85.8
	30.8		74.3
clinoenstatite ($MgSiO_3$)	39.3		28.2
	34.5		28.2
	32.3		21.6
	26.3	larnite (Ca_2SiO_4)	117.3
	18.0		113.3
	15.0		108.8
			106.3

[a] All reported values are parts per million from the oxygen-17 resonance in $H_2{}^{17}O$. Errors in all measurements are ±0.5 ppm.

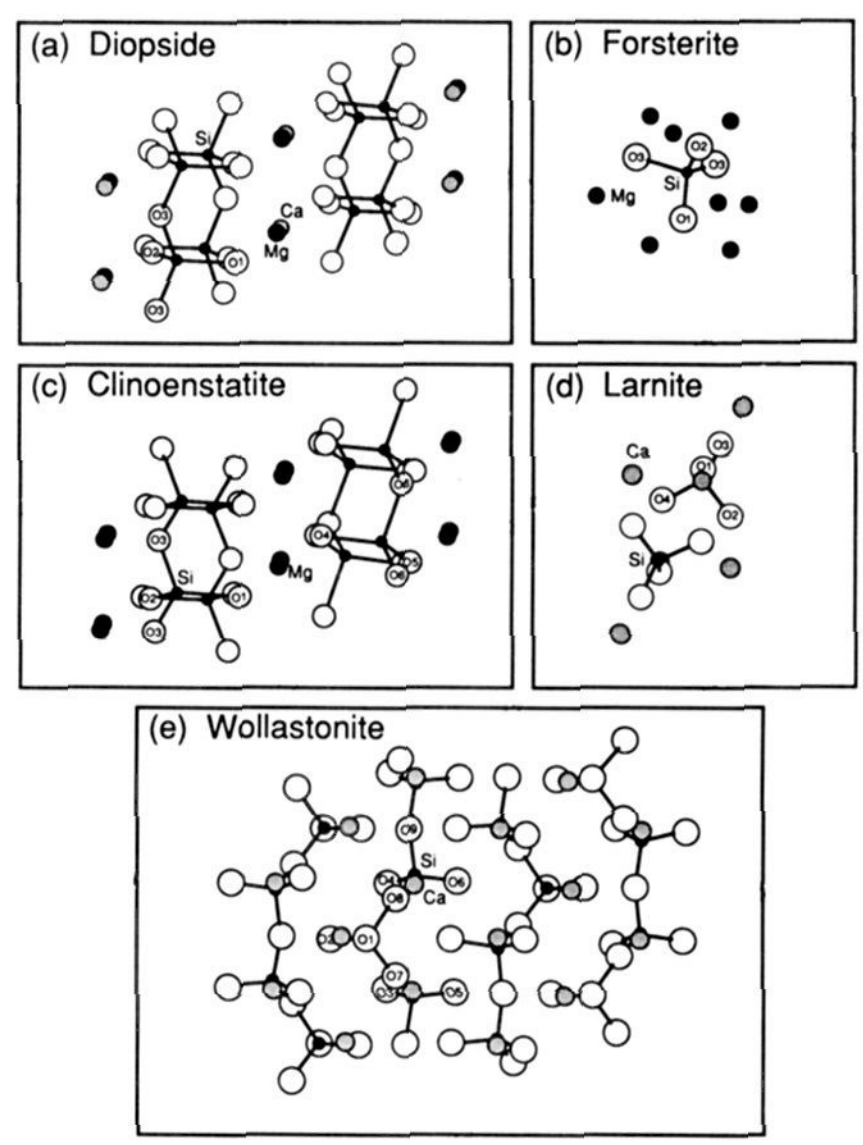

Figure 6. Structures of the five silicates enriched in oxygen-17 for this study. The magnesium and calcium species are offset in a and c to allow all cation sites to be seen. Numbering of the oxygens distinguishes the crystallographically inequivalent sites in each structure.

(36) Stebbins, J. Unpublished results.

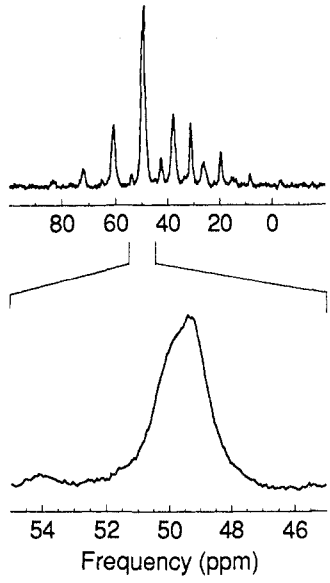

Figure 7. Expansion of the forsterite DOR spectrum in Figure 5, with a shoulder indicating two resonances around 49 ppm.

as clinoenstatite is also consistent with the position of the peak in the oxygen-17 spectra.

The DAS and DOR spectra of clinoenstatite are consistent with a crystal structure having six inequivalent oxygens in the unit cell,[37] four that are terminal sites and two that bridge adjacent silicate tetrahedra (see Figure 6c). The sidebands in the DOR spectrum, arising from the motion of the larger rotor, make identification of the upfield resonances difficult; the higher spinning speeds in the DAS experiment permit an unambiguous assignment. Previous interpretations,[33] based solely on static spectra, allowed for only three inequivalent oxygens. The small spread in the total shifts and similar quadrupolar parameters cause similar sites to be indistinguishable using lower resolution techniques, and this can also cause errors in the simulations of the spectra used to extract chemical shift and quadrupolar parameters. We assign the two less intense resonances at 18 and 15 ppm to bridging oxygen species O3 and O6 in Figure 6c, as the spread of the signal into more sidebands and less isotropic peak intensity is a signature of a larger quadrupolar coupling constant. For these bridging sites, there is poor agreement between the measured shifts and the calculated shift of 7 ppm based on earlier measurements.

For more complicated silicate species, such as the wollastonite, structural characterization by use of MAS alone is essentially impossible. The polytype parawollastonite, shown in Figure 6e, contains nine distinct oxygen sites.[38] One-dimensional DAS and DOR results show eight assignable oxygen-17 resonances for this particular silicate. As explained in the following text, two-dimensional data analysis helps to locate the ninth spectral line that overlaps with another resonance at 28.2 ppm, as well as allowing preliminary assignment of the upfield resonances to the three bridging oxygens (O7, O8, and O9 in Figure 6e).

Finally, the larnite structure in Figure 6d shows four distinct oxygen nuclei surrounding a central silicon atom with slightly different cation coordinations at each site.[39] The MAS spectrum is much narrower for larnite than for the other minerals, and the observed shifts for the distinct oxygens are much closer together. Four resonances are seen in the high-resolution DAS and DOR spectra of larnite in Figure 5. Additional broadening of the DAS lines compared to the DOR resonances is noticeable in all of the spectra presented, but it is most evident in the narrow spread of oxygen-17 resonance frequencies from larnite. Relaxation to other magnetic sublevels ($m \neq \pm^1/_2$) during the rather long flipping

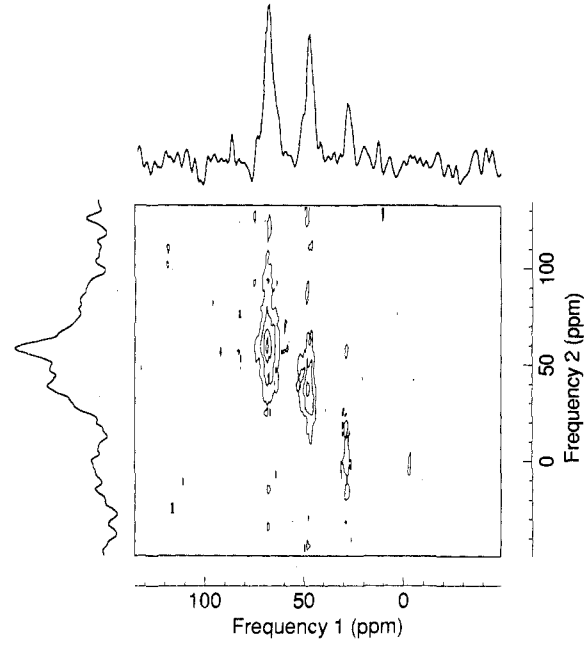

Figure 8. Two-dimensional DAS spectrum of oxygen-17 in diopside at 9.4 T. The time t_1 is the evolution time up until the refocusing of the anisotropic frequency contributions, and t_2 is the time period of the decay after the echo point. The time domain data matrix of 256 by 512 complex points was Fourier transformed with 40-Hz Lorentzian broadening in the first frequency dimension and 250 Hz in the second dimension.

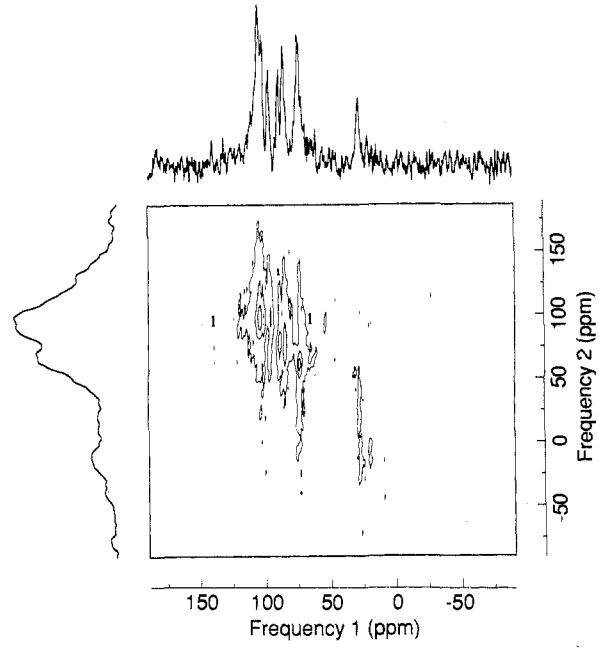

Figure 9. Two-dimensional DAS spectrum of oxygen-17 in wollastonite at 9.4 T.

time between the two DAS angles can lead to additional broadening in the DAS spectrum compared to the continuous DOR experiment.

The DAS experiments involve two time dimensions in a natural way, and two-dimensional Fourier transformation of the data can correlate the isotropic peaks along the high-resolution frequency axis with the spectra obtained while spinning at θ_2. Results for diopside, wollastonite, and clinoenstatite are presented in Figures 8–10. Patterns that overlap in conventional one-dimensional spectra are now separated in a two-dimensional display. With diopside, for example, slices integrated over the line shape at the isotropic frequencies in the first dimension parallel to the second frequency axis are shown in Figure 11. Simulations of line shapes with the quadrupolar parameters and isotropic chemical shifts from

(37) Morimoto, N.; Appleman, D. E.; Evans, H. T., Jr. *Z. Kristallogr.* **1960**, *114*, 120–147.
(38) Trojer, F. J. *Z. Kristallogr.* **1968**, *127*, 291–308.
(39) Midgely, C. M. *Acta Crystallogr.* **1952**, *5*, 307–312.

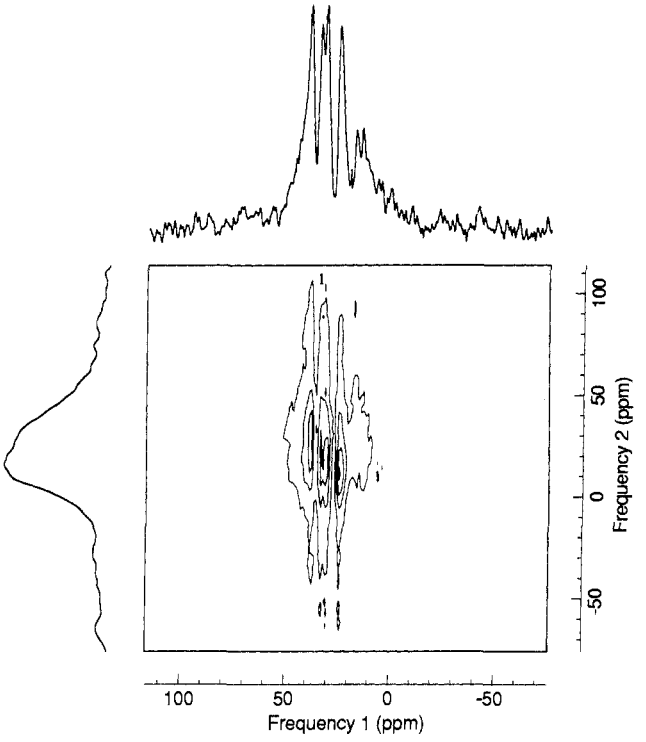

Figure 10. Two-dimensional DAS spectrum of oxygen-17 in clinoenstatite at 9.4 T.

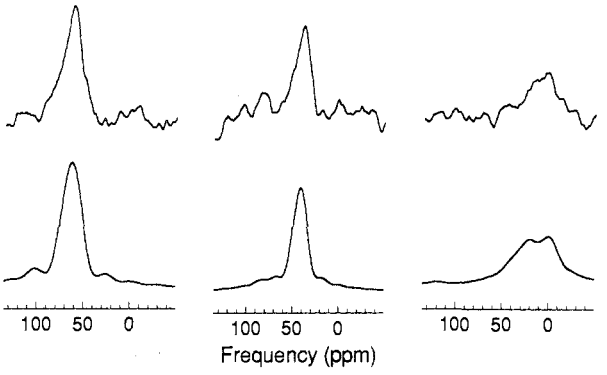

Figure 11. One-dimensional integrated slices through the two-dimensional DAS spectrum of diopside. The simulations (bottom) use the parameters from ref 33 (see Table II) and include approximately 20 ppm of line broadening.

Table II match these patterns closely. It must be stressed that these spectra represent absolute value line shapes obtained while spinning the sample at an angle of 79.2°. The chemical shift anisotropy and dipolar interactions present under these conditions lead to additional line broadening, which has been taken into consideration here only through additional exponential broadening of the calculated time-domain signals for each particular site.

A similar slice through the wollastonite DAS spectrum of Figure 9 reveals the power of using the second dimension to make spectral assignments. The resonance at 28.2 ppm in the first frequency dimension appears to arise from two resonances in the second dimension, which would occur as an overlap of two powder patterns. Spectral features present in the 28.2 ppm slice indicate two resonances with quadrupolar coupling constants in the range of 4–5 MHz, typical of bridging oxygen sites. The integrated intensity is also twice that of the isotropic resonance at 21.6 ppm, which we assign to the third distinct bridging oxygen in the structure. With these assignments, the resonances from all nine crystallographically distinct oxygens are tentatively identified.

More complicated structures, such as those found in larnite, clinoenstatite, and wollastonite, require careful analysis of the two-dimensional DAS data to extract the quadrupolar and chemical shift parameters. Preliminary fits using the second frequency dimension in the two-dimensional spectra of clinoenstatite and wollastonite provide approximate parameters, but more precise fits are still difficult. In particular, the broad lines from the bridging oxygen resonances in both species suffer from a poor signal to noise ratio.

In clinoenstatite, the four nonbridging oxygens all have similar quadrupolar parameters, with quadrupolar coupling constants of approximately 3.3 MHz (±0.1 MHz) and an η between 0.0 and 0.1. The isotropic second-order quadrupolar shift will be on the order of −22 ppm, yielding isotropic chemical shift contributions of 61, 57, 54, and 48 ppm for the four nonbridging sites. The two upfield resonances have couplings of about 4.0 MHz, while the asymmetry parameter is approximately 0.3 (±0.1). Therefore, chemical shift assignments for these two bridging oxygens are 52 and 49 ppm.

Upon examination of the second frequency dimension in Figure 9, the six downfield wollastonite resonances are also found to have similar quadrupolar parameters. The coupling constant is estimated at 2.3 MHz, and η is close to 0.1. The calculated second-order shift is −11 ppm, and the isotropic chemical shifts for these six nonbridging sites range from 85 to 114 ppm.

The two overlapping resonances from the bridging species in wollastonite have more than a chemical shift difference, as the second-order quadrupolar shift must also change if the total shift is to be the same. While the dependence of the second-order shift on the asymmetry parameter η is weak, the positions of the singularities exhibit a strong dependence upon η. This complicates the analysis, so that no tentative parameter assignments have been made. The wollastonite resonance at 21.6 ppm also has such low intensity that assignment of quadrupolar parameters is not currently possible. The use of pure-phase DAS spectra correlated with MAS powder patterns in the second dimension[31] should prove useful for final analysis of these three resonances, as line broadening from chemical shift anisotropy and dipolar interactions will be reduced. As a further measure of the quadrupolar and shielding parameters, obtaining spectra at two different field strengths and solving sets of equations in the form of eqs 5 and 6 can be useful in separating the chemical shift from the quadrupolar contributions.

To summarize, in the past, sharp NMR spectra from spin-$^1/_2$ nuclei such as silicon-29 have been useful in studying local bonding parameters in solids. Equally useful resolution is now available from quadrupolar nuclei, including oxygen-17. In this paper, we have outlined the techniques of DAS and DOR and illustrated the enhanced resolution possible in a class of oxygen-17 enriched minerals. Resolved resonances have been observed from samples with up to nine crystallographically distinct oxygen sites. In DAS, two-dimensional spectral analysis is used for correlating isotropic chemical shifts with quadrupolar parameters (C_Q and η) at each oxygen site. In DOR, a technically more demanding experiment, one-dimensional spectra can be accumulated directly.

Acknowledgment. We thank G. C. Chingas, J. Sachleben, T. Tammer, D. Colomb, C. Gaskins, and D. Murai for experimental assistance and probe construction. K.T.M. is an NSF Graduate Fellow, and B.F.C. acknowledges support as an NSF Postdoctoral Fellow in Chemistry. J.S. has received funding under NSF Grant No. NSFEAR05188. This work was supported by the Director, Office of Energy Research, Office of Basic Energy Sciences, Materials Science Division, of the U.S. Department of Energy under Contract No. DE-AC03-76SF00098.